Cation and Spin Ordering in the $n = 1$ Ruddlesden−Popper Phase $La_2Sr_2LiRuO_8$

Jennifer A. Rodgers,[†] Peter D. Battle,*[,†] Nicolas Dupré,[‡] Clare P. Grey,[‡] and Jeremy Sloan[†]

Inorganic Chemistry Laboratory, Oxford University, South Parks Road, Oxford, OX1 3QR, U.K., and Department of Chemistry, State University of New York at Stony Brook, Stony Brook, New York 11794-3400

Received June 14, 2004

The synthesis and characterization of a polycrystalline sample of the $n = 1$ Ruddlesden−Popper phase $La_2Sr_2LiRuO_8$ are reported. X-ray and neutron diffraction show that the six-coordinate sites are occupied by 1:1 ordered *xy* layers of Li:Ru, and the nine-coordinate sites are occupied by 1:1 ordered layers of La:Sr; a low concentration (7.4%, 9.8% respectively) of anti-site defects was detected on each sublattice. These layers stack in an ordered sequence along *z*, resulting in an orthorhombic unit cell with $a = 5.46001(1)$, $b = 5.45803(1)$, and $c = 25.5410(2)$ Å (space group *Imm*2) at 290 K. The structure is confirmed by high-resolution transmission electron microscopy, although the presence of stacking faults is revealed. ^{7}Li MAS NMR spectra are consistent with the diffraction data and show that the anti-site defects are not randomly distributed but occur in domains. The sample undergoes a transition to an antiferromagnetic phase at 85 K, with an ordered magnetic moment of 1.58(7) μ_B per Ru^{5+} aligned along [001]. The spins associated with the anti-site Ru cations freeze as a spin glass.

Introduction

To rationalize the electronic properties observed in a wide range of mixed-metal oxides, it is necessary to understand the interactions that occur between transition-metal cations with partially filled d shells. In many cases, including high-temperature superconductors and magnetoresistive manganates, the complexity of the system is partly attributable to the fact that the cations involved do not all have the same electron configuration, and partly to the existence of significant interactions between next-nearest-neighbors in addition to those between nearest-neighbors. The consequences of the presence of competing interactions in a mixed cation array depend on whether the different cations occur in an ordered or a disordered array; in general, the ordered case is easier to understand. It has also been shown that the electronic properties of these materials correlate with the degree of disorder on any sublattice of non-transition elements.[1] Ruddlesden−Popper (RP) oxides having the general formula $A_{n+1}B_nO_{3n+1}$ have been central to recent research in this area, and the $n = \infty$ perovskite phases have been studied in considerable depth. In this case, it is relatively easy to induce ordering among two cation species on the six-coordinate B-sites, although ordering among different cations on the A-sites is less common. We have previously[2,3] attempted to improve our understanding of the properties of $n = 1$ and $n = 2$ manganate phases by using cation ordering to reduce the number of competing interactions. Our strategy was to produce a 1:1 ordered arrangement of Li^+ and either Mn^{3+} or Mn^{4+}, thus simplifying the system by eliminating the nearest-neighbor (∼3.9 Å) Mn−Mn interaction. However, the difference in size and charge between the chosen cation pairs was not great enough to induce long-range, 3D cation ordering, although we saw strong evidence for 2D ordering in the perovskite sheets which lie perpendicular to the [001] axis of the tetragonal $n = 1$ and $n = 2$ RP structures. The lack of long-range ordering for $n = 1$ was perhaps not surprising in view of the results of previous studies of related systems. Abbattista et al.[4] have reported 1:1 chess-board ordering of Au and Li in $La_2Au_{0.5}Li_{0.5}O_4$, although more recent work[5] has suggested that this composition takes the T′ structure of Nd_2CuO_4.[6] A recent study by Warda et al.[7] of the compounds $La_2Li_{0.5}M_{0.5}O_4$ (M = Co, Ni, Cu) resulted in a model involving the twinning of two ordered domains; each domain contains ordered perovskite sheets perpendicular to [001], but the sheets stack along [001] in one of two orthogonal schemes. Consequently, the degree of ordering measured in an X-ray diffraction

* To whom correspondence should be addressed. E-mail: peter.battle@chem.ox.ac.uk.
[†] Oxford University.
[‡] State University of New York at Stony Brook.

(1) Williams, A. J.; Sobotka, B. M.; Attfield, J. P. *J. Solid State Chem.* **2003**, *173*, 456.
(2) Battle, P. D.; Burley, J. C.; Gallon, D. J.; Grey, C. P.; Sloan, J. *J. Solid State Chem.* **2003**, *177*, 119.
(3) Burley, J. C.; Battle, P. D.; Gallon, D. J.; Sloan, J.; Grey, C. P.; Rosseinsky, M. J. *J. Am. Chem. Soc.* **2002**, *124*, 620.
(4) Abbattista, F.; Vallino, M.; Mazza, D. *J. Less-Common Met.* **1985**, *110*, 391.
(5) Pietzuch, W.; Warda, S. A.; Massa, W.; Reinen, D. *Z. Anorg. Allg. Chem.* **2000**, *626*, 113.
(6) Muller-Buschbaum, H.; Wollschlager, H. *Z. Anorg. Allg. Chem.* **1975**, *414*, 76.
(7) Warda, S. A.; Pietzuch, W.; Berghofer, G.; Kesper, U.; Massa, W.; Reinen, D. *J. Solid State Chem.* **1998**, *138*, 18.

10.1021/cm049053w CCC: $27.50
Published on Web 10/01/2004

experiment depends on the relative values of the coherence length of the radiation and the typical linear dimension of the domains; the composition having M = Ni was described as 74% ordered, two different crystals with M = Co showed 35% and 48% order, and data from a crystal with M = Cu could only be analyzed when the Cu/Li distribution was assumed to be completely disordered. This description of the $La_2Li_{0.5}M_{0.5}O_4$ system is largely consistent with our own study of La_4LiMnO_8 and $La_3SrLiMnO_8$[3] and demonstrates that, although 2D ordering is easily induced, long-range 3D cation ordering on the B-sites of $n = 1$ RP phases is not readily achieved. A similar conclusion can be drawn[8] for $n = 2$ systems, but we shall not detail the evidence here. In an attempt to overcome the reluctance of $n = 1$ and $n = 2$ RP phases to show cation ordering, we have attempted to synthesize compositions in which the B-sites are occupied by a 1:1 ratio of Li^+ and Ru^{5+}, the idea being to use the greater difference in formal charge to drive the ordering; this strategy is known to work in the $n = \infty$ phase La_2LiRuO_6.[9] We describe below the synthesis and characterization of the $n = 1$ compound $La_2Sr_2LiRuO_8$; the results of our work on $n = 2$ phases will be described elsewhere. We attempted to increase the number of compositions in the present study by making many of the standard substitutions of solid-state chemistry, for example, Sr/Ba and La/Ln where Ln = Pr or Nd, but the sample quality deteriorated markedly when only 10% Ba was introduced, and no other lanthanide cation would stabilize the phase. The composition $La_2Sr_2LiRuO_8$ clearly contains a 1:1 ratio of two different cations on the A-site as well as the B-site. A-site ordering is also rare in these phases, although $NaLnTiO_4$ and $KLnTiO_4$[10−12] have both been shown to contain A-site layers ordered along [001] in the sequence −Ln−Ln−Na/K−Na/K−Ln−Ln−. We shall show below that $La_2Sr_2LiRuO_8$ contains an ordered Li/Ru array on the B-sites and an ordered La/Sr array on the A-sites. The ordering schemes observed at both sites differ from those that have been found previously. The antiferromagnetic structure adopted at low temperatures is consistent with the presence of an ordered cation array.

Experimental Section

A polycrystalline sample of $La_2Sr_2LiRuO_8$ was synthesized from spectroscopic grade reagents using standard high-temperature solid-state techniques. Stoichiometric quantities of $SrCO_3$, La_2O_3, and RuO_2 were ground together with an excess of volatile Li_2CO_3. The mixture was heated in an alumina crucible at 800 °C for 4 h, reground, and then fired as a loose powder at 900 °C for 17 h. The progress of the reaction was monitored by X-ray powder diffraction, and it was deemed to be complete when the diffraction pattern associated with the principal product did not change on further heating. X-ray data suitable for quantitative Rietveld[13] analysis were collected at room temperature in Bragg−Brentano geometry on a Siemens D5000 diffractometer operating with Cu $K\alpha_1$ radiation. The pattern was recorded over the angular range $10 \le 2\theta/° \le 120$ with a stepsize $\Delta 2\theta = 0.02°$. Neutron powder diffraction data were collected at 290 and 2 K on the time-of-flight (TOF) diffractometer POLARIS at the ISIS neutron source, Rutherford Appleton Laboratory. All of the diffraction data were analyzed by the Rietveld method as implemented in the GSAS[14] program suite.

Magic-angle-spinning (MAS) ^7Li NMR experiments were performed at an operating frequency of 77.79 MHz, on a CMX-200 spectrometer. Spectra were acquired with a spinning frequency (ω_r) of 30 kHz with a probe built by A. Samoson and co-workers (National Institute of Chemical Physics and Biophysics, Tallinn, Estonia), equipped with 2 mm rotors, by using a rotor synchronized echo sequence ($90°-\tau-180°-\tau-$acq.), where $\tau = 1/(\omega_r)$. A $\pi/2$ pulse width of 2.1 μs for ^7Li on the CMX-200 spectrometer was used, with a pulse delay of 0.2 s. Spectra were acquired at room temperature (i.e., with no control of the temperature); this corresponds to a sample temperature of between 60 and 70 °C.

Electron diffraction patterns and high-resolution lattice images were recorded on JEOL 4000EX and 3000F transmission electron microscopes operating at 400 and 300 kV with $C_s = 1$ and 0.6 mm, respectively. Image simulations based on the structures derived by X-ray and neutron diffraction were performed using Java EMS[15] and SimulaTEM software packages[16] and the instrumental parameters specified above.

Magnetometry was performed using a Quantum Design MPMS SQUID magnetometer. The sample magnetization was measured as a function of temperature on warming in an applied field of 100 Oe after cooling the sample to 5 K in either zero field (ZFC) or the measuring field (FC). The field dependence of the magnetization was measured over the range $-50 \le H/\text{kOe} \le 50$ at selected temperatures; the sample was cooled to the measurement temperature in a field of 50 kOe.

Results

The widths of the Bragg peaks in the X-ray diffraction pattern of the reaction product were narrow enough (fwhm ≈ 0.1°) to suggest that the reaction product was highly crystalline. All of the peaks could be indexed using a body-centered orthorhombic unit cell with lattice parameters corresponding to a $\sim\sqrt{2} \times \sim\sqrt{2} \times \sim 2$ expansion of the unit cell usually associated with the tetragonal $n = 1$ Ruddlesden−Popper structure. No other phases were apparent in the X-ray data. After a number of possible structural models were screened, it became clear that the X-ray data were best modeled by the composition $La_2Sr_2LiRuO_8$ in an $n = 1$ structure which is built up of layers of RuO_6 and LiO_6 octahedra which share vertices in a 1:1 chess-board arrangement,

(8) Rodgers, J. A. D. Phil Thesis, Oxford, 2004.
(9) Battle, P. D.; Grey, C. P.; Hervieu, M.; Martin, C.; Moore, C. A.; Paik, Y. *J. Solid State Chem.* **2003**, *175*, 20.
(10) Toda, K.; Kameo, Y.; Kurita, S.; Sato, M. *J. Alloys Compd.* **1996**, *234*, 19.
(11) Schaak, R. E.; Mallouk, T. E. *J. Solid State Chem.* **2001**, *161*, 225.
(12) Byeon, S. H.; Park, K.; Itoh, M. *J. Solid State Chem.* **1996**, *121*, 430.
(13) Rietveld, H. M. *J. Appl. Crystallogr.* **1969**, *2*, 65.
(14) Larson, A. C.; von Dreele, R. B. General Structure Analysis System (GSAS), Report LAUR 86-748 Los Alamos National Laboratories, Los Alamos, NM, 1990.
(15) Stadelmann, P. 1995, http://cimesg1.epfl.ch/CIOL/asu94/ICT_1.html.
(16) Gomez, A.; Beltran-del-Rio, L. *Rev. Latinoam. Metal. Mater.* **2001**, *21*, 46.

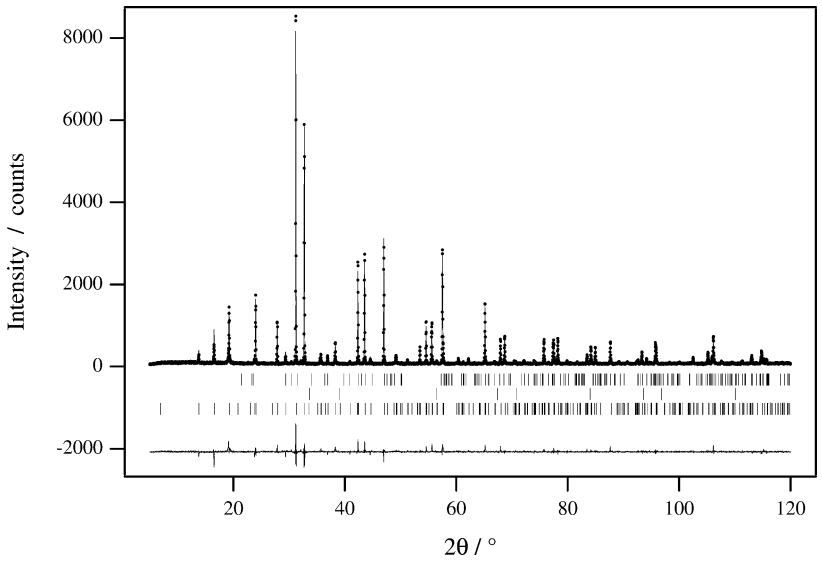

Figure 1. Observed (●), calculated (−), and difference X-ray diffraction profiles for $La_2Sr_2LiRuO_8$ at room temperature. The upper, central, and lower ticks mark the reflection positions for Li_2CO_3, Li_2O, and $La_2Sr_2LiRuO_8$, respectively.

thus expanding the unit cell in the *xy* plane. The doubling of the unit cell along the *z* axis is caused by the ordered stacking of the layers in this direction. The unit cell expansion also reflects the ordering of Sr and La over the nine-coordinate sites in the rock-salt layers. This structure can be described in space group *Imm*2. The neutron diffraction data could also be accounted for using this model, although weak contributions from lithium carbonate and lithium oxide were also apparent. The structure was refined by a simultaneous analysis of the X-ray and neutron data, the latter comprising three diffraction patterns recorded on the POLARIS detectors at $2\theta = 145°$, 90°, and 30°. The *z* coordinate of one atom was held fixed to define the origin of the unit cell. Trial refinements found no evidence of vacancies on the oxide sublattice, which was consequently constrained to be fully occupied. The degree of cation ordering on both the La/Sr and the Li/Ru sublattices was allowed to vary. Preliminary refinements used isotropic displacement parameters, but it became clear that the scattering from the axial oxide sites coordinated to Li was better modeled when anisotropic displacement parameters were used. The displacement parameters of the Li/Ru sites were held at zero, and all others were refined isotropically in the final refinements. The best fits between the observed and calculated X-ray and neutron diffraction profiles are presented in Figures 1 and 2. The refined unit cell and structural parameters are listed in Tables 1 and 2, and bond lengths and bond angles are given in Table 3. A polyhedral representation of the structure is drawn in Figure 3, the local environment of the Li and Ru cations is shown in Figure 4, and the key anisotropic displacement parameters are illustrated in Figure 5. Trial refinements based on the related T′ structure, which is adopted by some A_2BO_4 phases, were unsuccessful.

Support for a structural model in which the Li and Ru cations are ordered comes from the NMR data shown in Figure 6. The ^{7}Li NMR spectrum is dominated by two overlapping resonances at −350 and −375 ppm, consistent with the two lithium local environments identified from the diffraction data. The large NMR shifts are ascribed to a hyperfine interaction[3,9,17] which involves the transfer of unpaired spin density from Ru^{5+} to the 2s Li orbital, via the intervening oxygen orbitals. Only the paramagnetic Ru^{5+} ($4d^3$) ions contribute to the hyperfine shift, as all of the other ions are diamagnetic. Previous studies on lithium ruthenium (V) oxide and the isoelectronic lithium manganese (IV) oxides showed that the contribution to the hyperfine shift from each Li−O−M (M = Mn/Ru) interaction is additive, the total hyperfine shift depending on the number of Li−O−M bonds and the Li−O−Mn bond angles. A negative hyperfine shift arises from the overlap between an empty Ru/Mn e_g orbital, an oxygen 2p orbital, and the Li 2s orbital. This overlap is maximized for a "180° interaction", that is, for a Li−O−M bond angle of 180°, with a decrease in the Li−O−Ru/Mn bond angle from 180° resulting in a decrease in the size of the hyperfine interaction. Both Li1 and Li2 are connected to four nearby Ru^{5+} ions via four Li−O−Ru bonds, with bond angles of 177.9° and 169.9° for Li2 and Li1, respectively. Thus, the resonances at −375 and −350 ppm are assigned to Li2 and Li1, respectively, single Li−O−Ru interactions with bond angles of 177.9° and 169.9° resulting in shifts of −94 and −87.5 ppm, respectively. These ^{7}Li NMR shifts are consistent with the shift observed for the ordered perovskite Li_2LiRuO_6 (−33 ppm), which contains Li^+ ions connected to six Li−O−Ru^{5+} bonds with much smaller bond angles of 154.3−155.6°.[9] The shifts are also of the same order of magnitude as the estimated shifts for the 180° interactions in Li_3RuO_4.[18] The small number of resonances in the spectrum is consistent with an ordered structure, as a random distribution of Li^+ and Ru^{5+} ions in the perovskite layers would lead to a larger number of local environments and a correspondingly larger number of resonances in the spectrum. Random Li−Ru distributions are predicted to result in intense ^{7}Li resonances at −262 to −282 ppm (3 Ru neighbors), −175 to −188 ppm (2 Ru neighbors), and between −87.5 and −94 ppm

(17) Lee, Y. J.; Wang, F.; Grey, C. P. *J. Am. Chem. Soc.* **1998**, *120*, 12601.
(18) Alexander, A.; Battle, P. D.; Burley, J. C.; Gallon, D.; Grey, C. P.; Kim, S. H. *J. Mater. Chem.* **2003**, *13*, 2612.

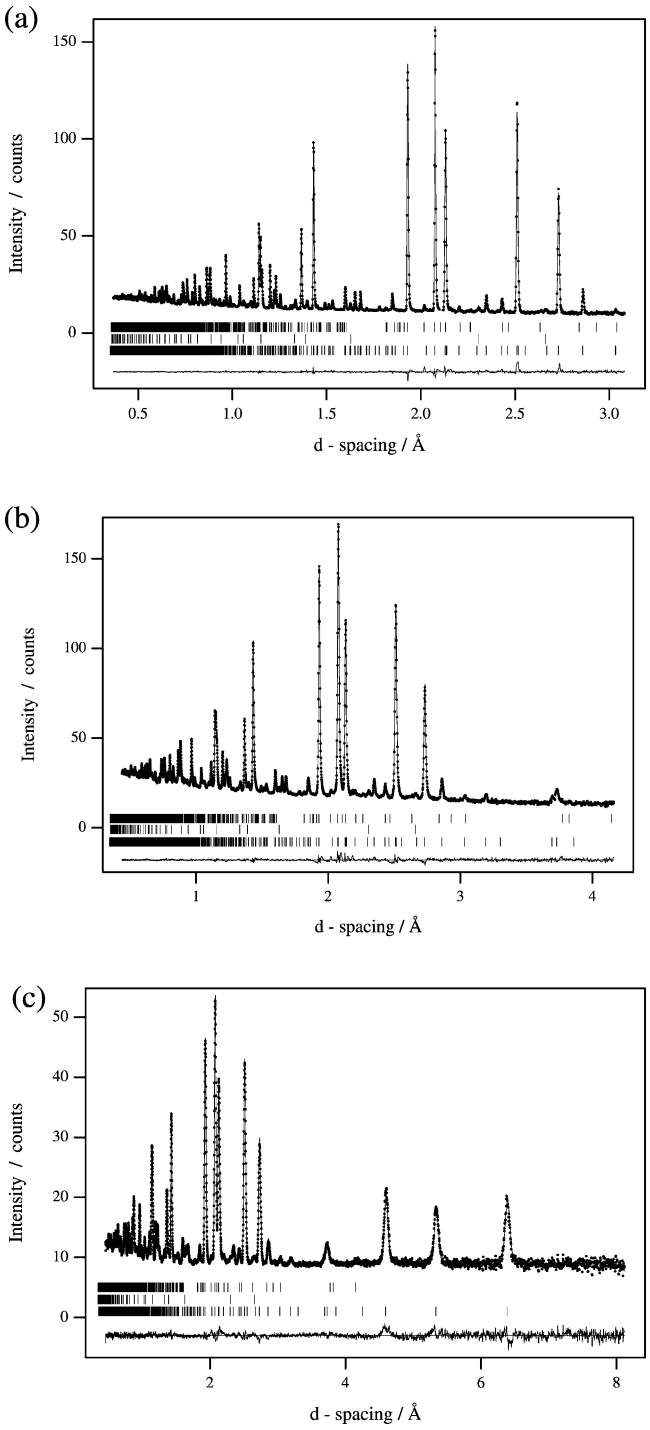

Figure 2. Observed (●), calculated (−), and difference neutron diffraction profiles for $La_2Sr_2LiRuO_8$ at room temperature and (a) $2\theta = 145°$, (b) $2\theta = 90°$, and (c) $2\theta = 30°$. The upper, central, and lower ticks mark the reflection positions for Li_2CO_3, Li_2O, and $La_2Sr_2LiRuO_8$, respectively.

Table 1. Unit Cell Dimensions for $La_2Sr_2LiRuO_8$, Space Group *Imm*2

	290 K	2 K
a (Å)	5.46001(1)	5.4507(3)
b (Å)	5.45803(1)	5.4526(3)
c (Å)	25.5410(2)	25.5095(1)
V (Å^3)	761.28(1)	758.15(5)

(1 Ru neighbor), environments with 2 Ru nearest neighbors being the most probable. This prediction is not consistent with the experimental spectrum. However, the weaker resonance at approximately −274 ppm can be assigned to the local environment containing 3 Ru ions. Deconvolution and integration of the different resonances led to an intensity ratio of close to 1:1 for the signals at −350 and −375 ppm, consistent with their assignment to Li1 and Li2. The resonance at −274 ppm represents only 3% of the total signal intensity and is consistent with the strongly ordered structure of $La_2Sr_2LiRuO_8$. The resonance at 0 ppm, corresponding to a diamagnetic impurity (or possibly a local environment in $La_2Sr_2LiRuO_8$ with 4 nearby Li ions and no Ru ions), represents approximately 2% of the total signal.

The resonances due to Li1 and Li2 have very different line widths, which must be related to slight differences in disorder surrounding these sites. Large atomic displacement ellipsoids are seen for the axial oxygen atoms coordinated to both Li1 and Li2 (Figure 5), consistent with disorder near both of these sites. Both sites are close to 4 La^{3+} and 4 Sr^{2+} ions, which are also subject to a small amount of La/Sr site exchange. Unfortunately, there was insufficient data to permit an independent refinement of the occupancies of the 8 La/Sr sites and the thermal parameters of the axial oxygen atoms coordinated to Li1/Li2. The NMR spectra suggest that there is a difference in the disorder surrounding the Li1 and Li2 sites, the Li1 site, with its smaller Li−O−Ru bond angles, being associated with larger disorder in its local coordination shell.

The electron diffraction pattern of the [010] zone shown in Figure 7 is consistent with the unit cell deduced from the X-ray, and the lattice image and simulation shown in Figure 8a are readily related to a polyhedral projection of the cation-ordered structure (Figure 8b). The through-focus series of images presented in Figure 9 provides further evidence of the validity of our model. However, the enlarged image shown in Figure 10 shows that the layer stacking along [001] is not perfect and that anti-site Li/Ru defects do occur. The presence of almost-continuous lines of scattering parallel to c* in the diffraction pattern shown in Figure 11 suggests that some crystallites are well ordered in the xy plane, but exhibit a considerable degree of stacking disorder in the perpendicular direction.

The temperature dependence of the molar magnetic susceptibility of $La_2Sr_2LiRuO_8$ is shown in Figure 12. The ZFC and FC susceptibilities overlie at temperatures above 90 K, but hysteresis is apparent below this temperature. The data were fitted to a Curie−Weiss law over the temperature range $125 \leq T/K \leq 300$, resulting in values of the Curie and Weiss constants of $C = 2.33(1)$ cm^3 K mol^{-1} and $\theta = -174(2)$ K, respectively; the former corresponds to an effective magnetic moment $\mu_{eff} = 4.31\ \mu_B$ per Ru. It can be seen from Figure 13 that the field dependence of the magnetization is not symmetrical about the origin at 5 K.

The majority of the reflections observed in the neutron diffraction pattern collected at 2 K were consistent with the structural model used in the analysis of the room-temperature data. However, a number of additional reflections were observed at high d-spacings at low temperature, suggesting that the sample shows long-range magnetic order. The additional Bragg peaks could be indexed with a $2a \times 2b \times c$ expansion of the structural unit cell. In the analysis of these data, the

Table 2. Atomic Parameters of $La_2Sr_2LiRuO_8$ at 290 and 2 K, Space Group *Imm*2[a]

			290 K	2 K
La/Sr:	La/Sr1 (0,0,*z*)	z	0.57079	0.57079
	La/Sr2 (0,0,*z*)	z	0.4315(3)	0.4301(4)
	La/Sr3 (0,$^1/_2$,*z*)	z	0.8200(3)	0.8186(3)
	La/Sr4 (0,$^1/_2$,*z*)	z	0.1805(4)	0.1799(5)
	occupancy 1−4		0.902(9)	0.902
	La/Sr5 (0,0,*z*)	z	0.0710(5)	0.0701(6)
	La/Sr6 (0,0,*z*)	z	0.9301(4)	0.9295(4)
	La/Sr7 (0,$^1/_2$,*z*)	z	0.6802(3)	0.6797(3)
	La/Sr8 (0,$^1/_2$,*z*)	z	0.3211(4)	0.3203(6)
	occupancy 5−8		0.098(9)	0.098
	U_{iso} (Å^2)	La/Sr1−La/Sr4	0.0050(2)	0.0020(2)
		Sr/La5−Sr/La8	0.0080(2)	0.0047(2)
Li/Ru:	Li/Ru1 (0,0,*z*)	z	0.2532(8)	0.256(1)
	Li/Ru2 (0,$^1/_2$,*z*)	z	−0.0106(4)	0.005(1)
	occupancy		0.926(2)	0.926
	Ru/Li3 (0,$^1/_2$,*z*)	z	0.4992(3)	0.4989(4)
	Ru/Li4 (0,0,*z*)	z	0.7493(3)	0.7492(4)
	occupancy		0.074(2)	0.074
	U_{iso} (Å^2)	Li/Ru1−Li/Ru2	0	0
		Li/Ru3−Li/Ru4	0	0
O:	O1	x	0.2485(8)	0.2450(8)
		y	0.256(1)	0.2469(6)
		z	0.5010(3)	0.5000(3)
	O2	x	0.2546(9)	0.2529(9)
		y	0.748(1)	0.743(1)
		z	0.2525(3)	0.2522(3)
	O3 (0,0,*z*)	z	0.6700(4)	0.6710(5)
	O4 (0,0,*z*)	z	0.8320(5)	0.8298(5)
	O5 (0,$^1/_2$,*z*)	z	0.4215(4)	0.4193(6)
	O6 (0,$^1/_2$,*z*)	z	0.5801(3)	0.5809(6)
	O7 (0,$^1/_2$,*z*)	z	0.0955(5)	0.0939(6)
	O8 (0,$^1/_2$,*z*)	z	0.9117(5)	0.9116(5)
	O9 (0,0,*z*)	z	0.3379(5)	0.3381(5)
	O10 (0,0,*z*)	z	0.1584(6)	0.1575(6)
	O1,O2	U_{iso} (Å^2)	0.00622(8)	0.00382(9)
	O3,O4	U_{iso} (Å^2)	0.0122(7)	0.0024(6)
	O5,O6	U_{iso} (Å^2)	0.0033(3)	0.009(1)
	O7,O8,O9,O10	U_{11} (Å^2)	0.038(3)	0.037(3)
	O7,O8,O9,O10	U_{22} (Å^2)	0.049(3)	0.046(4)
	O7,O8,O9,O10	U_{33} (Å^2)	0.0057(6)	0.0050(6)

[a] The fractional occupancies of the A-sites refer to the proportion of La occupying the site, and the fractional occupancies of the B-sites refer to the proportion of Li occupying the site. Wt % Li_2O = 0.379(8)%, wt % Li_2CO_3 = 0.26(2)%. GOF parameters for 290 K: χ^2 = 2.167, R_{wp} = 1.43, R_p = 5.79, 116 variables. For 2 K: χ^2 = 2.762, R_{wp} = 1.43, R_p = 2.44, 91 variables.

cation distribution and the concentrations of the impurity phases were held constant at the values deduced from the high temperature data, but the atomic coordinates and the displacement parameters were allowed to vary as described above. The absence of any significant decrease in the components of the anisotropic displacement parameters of O7, O8, O9, and O10 on cooling suggests that their relatively large values are attributable to static disorder rather than to large-amplitude thermal motion. The additional reflections were well modeled by a spin structure, shown in Figure 14, which involves antiferromagnetic alignment of nearest-neighbor Ru cations in the perovskite layers. The magnetic moments of the Ru cations were found to align along the *z* axis with a magnitude of 1.58(7) μ_B per Ru. The observed and calculated diffraction profiles in the high *d*-spacing region are shown in Figure 15.

Table 3. Bond Distances (Å) and Angles (deg) in $La_2Sr_2LiRuO_8$ at Room Temperature

La1−O1 (×4)	2.640(6)	Sr5−O1 (×4)	2.617(8)
La1−O3	2.54(1)	Sr5−O6 (×2)	2.740(1)
La1−O6 (×2)	2.7394(7)	Sr5−O7 (×2)	2.800(3)
La1−O7 (×2)	2.802(3)	Sr5−O10	2.23(1)
La2−O1 (×4)	2.637(6)	Sr6−O1 (×4)	2.634(7)
La2−O5 (×2)	2.7409(9)	Sr6−O4	2.51(1)
La2−O8 (×2)	2.777(2)	Sr6−O6 (×2)	2.7390(9)
La2−O9	2.39(1)	Sr6−O8 (×2)	2.770(2)
La3−O2 (×4)	2.579(6)	Sr7−O2 (×4)	2.664(7)
La3−O4 (×2)	2.746(1)	Sr7−O3 (×2)	2.741(1)
La3−O8	2.34(1)	Sr7−O6	2.56(1)
La3−O9 (×2)	2.768(2)	Sr7−O10 (×2)	2.786(3)
La4−O2 (×4)	2.674(6)	Sr8−O2 (×4)	2.615(6)
La4−O3 (×2)	2.743(1)	Sr8−O4 (×2)	2.744(1)
La4−O7	2.17(1)	Sr8−O5	2.56(1)
La4−O10 (×2)	2.787(3)	Sr8−O9 (×2)	2.762(2)
mean La−O[a]	2.7(1)	mean Sr−O[a]	2.6(4)
Li1−O2 (×4)	1.955(5)	Ru1−O1 (×4)	1.901(4)
Li1−O9	2.16(2)	Ru1−O5	1.986(8)
Li1−O10	2.42(2)	Ru1−O6	2.066(9)
Li2−O1 (×4)	1.982(5)	Ru2−O2 (×4)	1.908(5)
Li2−O7	2.71(2)	Ru2−O3	2.03(1)
Li2−O8	1.99(2)	Ru2−O4	2.11(1)
mean Li−O	2.1(2)	mean Ru−O	1.95(7)
Li1−O1−Ru1	169.9(3)		
Li2−O2−Ru2	177.9(6)		

[a] 90.2(9)% of the sites are occupied by the specified La/Sr cation; the remainder are occupied by Sr/La.

Discussion

$La_2Sr_2LiRuO_8$ is unusual in a number of different ways. First, it is the only composition in the family $Ln_2Sr_{2-x}Ba_xLiRuO_8$ for which we were able to prepare a sample with an acceptable level of purity and crystallinity. It is also the first example of an n =1 RP phase to show cation ordering on both the A-sites and the

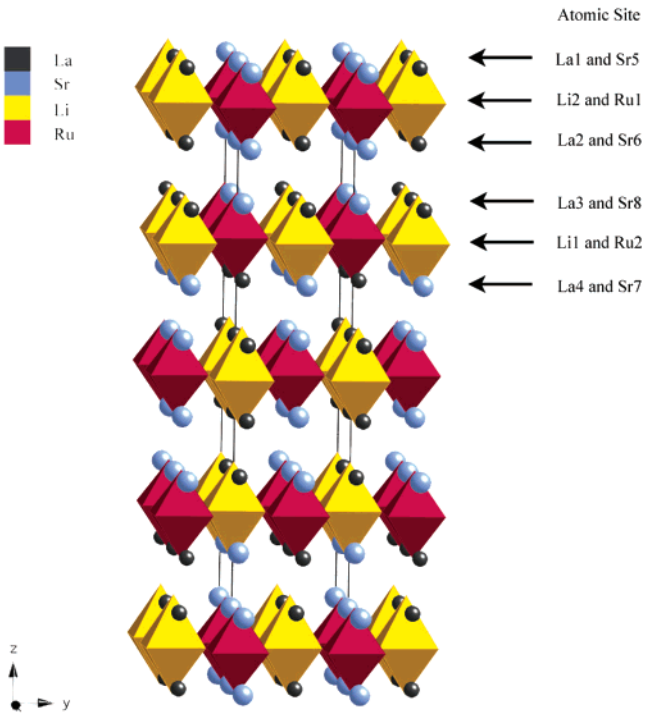

Figure 3. Polyhedral representation of the structure of $La_2Sr_2LiRuO_8$, space group *Imm*2.

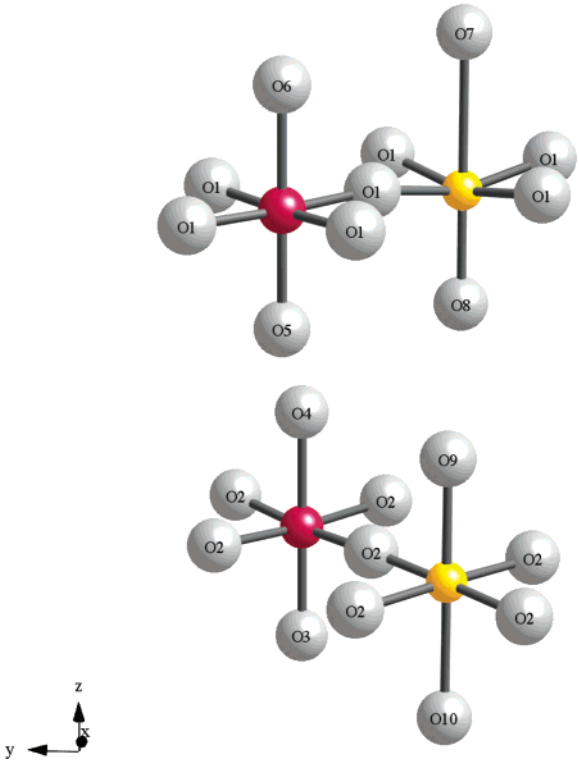

Figure 4. Representation of the LiO_6 and RuO_6 octahedra in $La_2Sr_2LiRuO_8$.

B-sites, and the first to show a pattern of cation ordering that necessitates a doubling of the unit cell parameter *c*. The B-site ordering scheme adopted was discussed as a possibility by Warda et al.[7] but has never previously been observed. Together, these observations suggest that the criteria for the stability of this structure are very narrow and that we were fortunate to discover this material. The formation of a phase with 3D cation ordering on the B-sites was one of the objectives of this study, and our results demonstrate that it is easier to observe order within a Li/Ru array than within the Li/Mn arrays studied previously. However, perhaps the most surprising aspect of the structure is the nearly complete ordering of the La^{3+} and Sr^{2+} cations on the A-sites. This would be less surprising in an $n = 2$[19] or $n = 3$[20] phase, where there are two chemically distinct A-sites (within the perovskite blocks and between the blocks), but in the $n = 1$ structure all of the sites are chemically equivalent and the long-range ordering of two cations with similar radii and a small charge difference is unexpected. There are certainly many $n = \infty$ perovskite compositions with a disordered arrangement of the same pair of cations on the single set of A-sites. Furthermore, the nature of the ordering, with mixed 1:1 La/Sr sheets, is different from that observed in other $n = 1$ phases which have an ordered A sublattice, for example, $NaLnTiO_4$.[12]

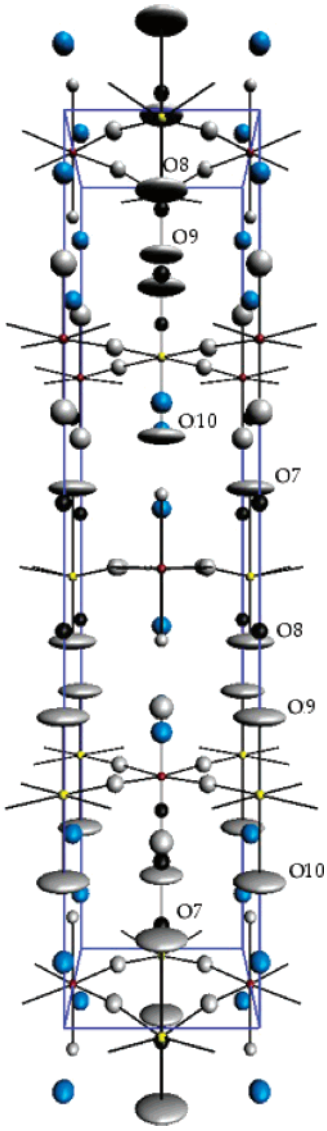

Figure 5. Atomic displacement ellipsoids (99%) for $La_2Sr_2LiRuO_8$ at room temperature derived from simultaneous Rietveld refinement of neutron and X-ray data.

(19) Battle, P. D.; Green, M. A.; Laskey, N. S.; Millburn, J. E.; Murphy, L.; Rosseinsky, M. J.; Sullivan, S. P.; Vente, J. F. *Chem. Mater.* **1997**, *9*, 552.
(20) Amow, G.; Greedan, J. E. *Acta Crystallogr.* **1998**, *C54*, 1053.

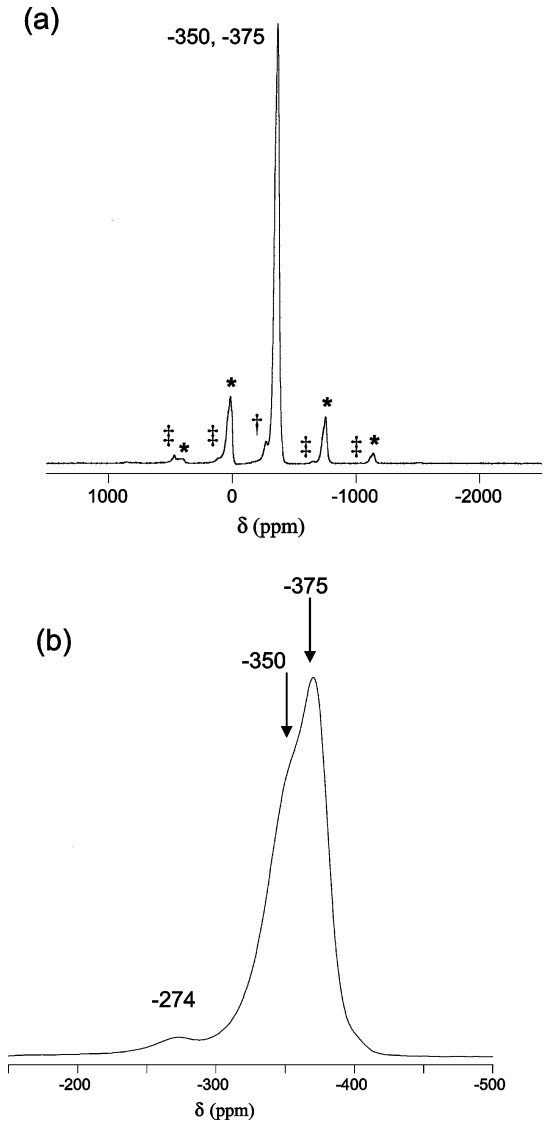

Figure 6. (a) ^{7}Li MAS NMR spectrum of $La_2Sr_2LiRuO_8$, acquired with a spinning speed of 30 kHz. Spinning sidebands of the main phase are indicated (∗). An additional resonance and related sidebands are labeled † and ‡, respectively. (b) Enlarged region of the ^{7}Li MAS NMR spectrum of $La_2Sr_2LiRuO_8$, with arrows highlighting the two distinct resonances of the main peak.

The overall level of agreement between the observed and calculated X-ray and neutron diffraction patterns, and hence the quality of our structural model, can be judged from Figures 1 and 2. The enlargement of the unit cell required to accommodate the ordering on both the A- and the B-sites leads to the presence of a relatively large number of atoms in the asymmetric unit, although many of them have only one free coordinate. The mean bond lengths around each site (Table 1) are chemically reasonable, and there is good agreement with the mean Li–O and Ru–O distances (2.08 and 1.95 Å, respectively) found in the perovskite La_2LiRuO_6. The shortest bond lengths around the La^{3+} and Sr^{2+} cations all involve oxide ions bonded axially to Li^+ cations, that is, those for which we have used anisotropic displacement parameters to model static disorder. The environment of the alkali-metal cations is highly distorted, being compressed in the *xy* plane and extended in an

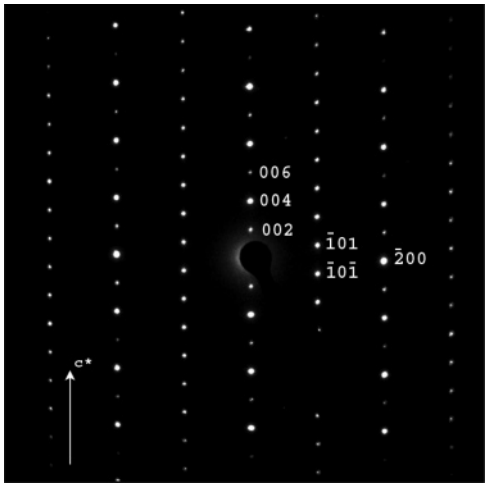

Figure 7. Selected-area electron diffraction pattern of the [010] zone of $La_2Sr_2LiRuO_8$.

asymmetric manner along *z*. As a result of the long Li2–O7 bond, the direct La4–O3 distance is reduced below the usual range of values, but the compression is relieved by the static displacement of O7 in the plane perpendicular to the bond. The other bonds to O7, involving Sr5 and La1, are long enough (~2.8 Å) to tolerate the resulting compression. The environment of the Ru^{5+} cations is also asymmetric along *z*, but to a lesser degree. The BO_6 octahedra in the $n = 1$ RP structure always show an axial distortion along [001], but the asymmetry observed in the present case is unusual, and more akin to the environment found in $n = 2$ phases. In both cases, it derives from the absence of a center of symmetry at the B-site.

The results of our electron microscopy experiments show that the layered structure of $La_2Sr_2LiRuO_8$ is subject to defect formation at the microstructure level. This is apparent in both lattice images (Figure 11) and electron diffraction patterns (Figure 12). The existence of these defects is reminiscent of our previous studies of $La_3SrLiMnO_8$ and La_4LiMnO_8 in which we were forced to analyze X-ray and neutron diffraction data in a space group that described the average structure over the relevant length scale, but did not accurately describe the local structure. This raises a question concerning the validity of our choice of *Imm*2 as the space group of $La_2Sr_2LiRuO_8$. It became clear during our initial analysis that this space group gave the best account of the cation ordering and the atomic positions in the average structure, but there are likely to be local structural variations which we have not modeled accurately. The static disorder about the oxide site axial to the Li^+ cations is one example, which may itself be related to the cation disorder observed on both the A (10%)- and B (7.5%)-sites. The ^{7}Li MAS NMR spectrum is consistent with our structural model in that it shows two strong resonances, with a small difference in chemical shift, which can be attributed to the Li1 and Li2 sites. The much weaker resonance at ~ −275 ppm might then be assigned to the Li3 and Li4 sites, that is, to the Li which is associated with anti-site defects. On the basis of the chemical shift of −274 ppm, this resonance was assigned to the local environment in which Li is surrounded by three Ru^{5+} ions in the perovskite layers, and this is the local environment created when one Ru^{5+} ion

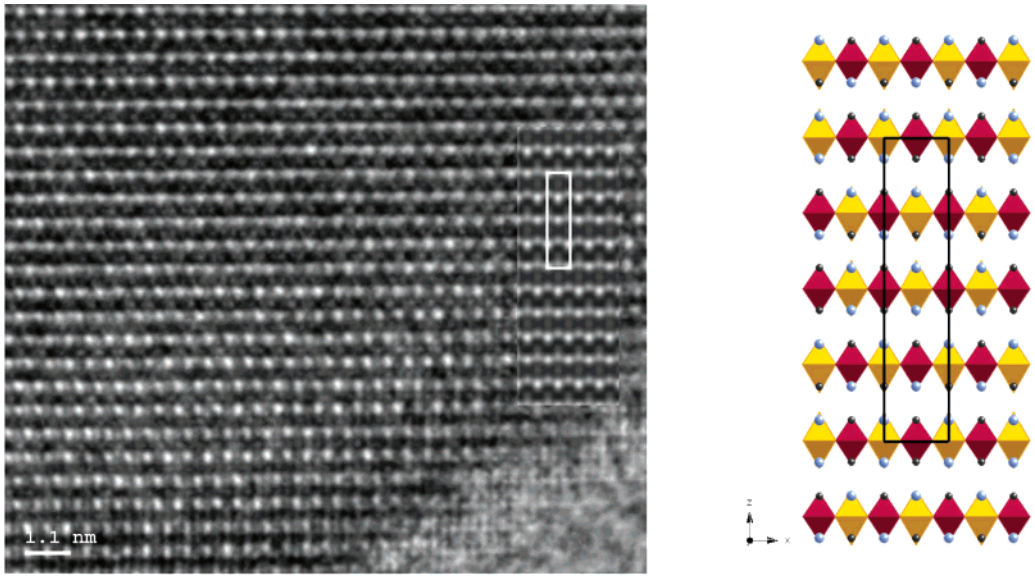

Figure 8. High-resolution [010] lattice image of $La_2Sr_2LiRuO_8$. The inset (right) depicts the simulated image at defocus 100 nm, thickness 6 nm with the unit cell outlined. (b) Polyhedral representation of the [010] zone for comparison with the image; the centers of the yellow octahedra can be related to the bright white spots in the lattice image.

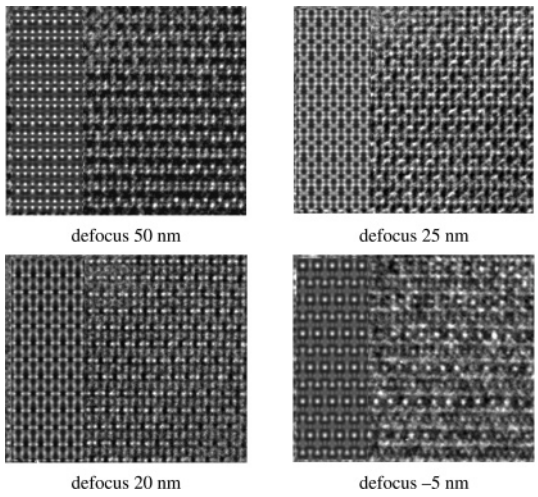

Figure 9. Selection of images from a through-focal series of $La_2Sr_2LiRuO_8$ in [010] projection. Simulations (inset to left of images) were produced using a crystal thickness of 6 nm.

neighboring either Li1 or Li2 is replaced by a Li^+ ion. Li^+ substitution on a Ru^{5+} site, without any substitution of the nearby Li sites by Ru^{5+}, also results in a Li^+ cation which is surrounded by Li^+ ions only and will give rise to a resonance at 0 ppm. The concentrations of the different Li local environments can be calculated on the basis of random occupancy of 7.5% of the Ru sites by Li, and 7.5% of the Li sites by Ru; 68%, 22%, and 2.5% of the Li ions occupy Li1/Li2 sites with 4, 3, and 2 Ru nearest neighbors (and give rise to ^{7}Li resonances at approximately −350 to −375 ppm (Li−4Ru), −262 to −282 ppm (Li−3Ru), and −175 to −188 ppm (Li−2Ru)), while 5% and 2% of the Li ions occupy Ru sites with 0 and 1 Ru nearest neighbors (^{7}Li resonances at approximately 0 (Li−0Ru) and −87.5 to −94 ppm (Li−1Ru)), respectively. The Li−3Ru local environment is predicted to occur in a much higher concentration (22%) than was seen experimentally (3%), indicating that a simple anti-site model, with random Li/Ru exchange, cannot account for the observed NMR spectra. Two possible defects are consistent with the data. The first consists of a large anti-site domain in the *xy* plane, with inverse Li/Ru distributions and strict Li−Ru alternation (and thus Li−4Ru and Ru−4Li local environments only). The −274 ppm resonance is then assigned to the boundaries between the domains, where the Li−3Ru environments are present. A domain wall running along the ⟨110⟩ directions will create such a local environment. The second possible defect involves a stacking fault in the [001] direction, involving a translation of an entire perovskite layer by $2^{1/2}(\mathbf{a} + \mathbf{b})$ in the ⟨110⟩ direction, maintaining strict Li−Ru alternation. These stacking faults will not affect the NMR spectrum significantly, because the hyperfine shifts are dominated by changes in the first and second cation coordination shells, but they will be seen by TEM. This defect must then be coupled with a small amount (approximately 0.075%) of Li/Ru exchange in the layers, to produce the ^{7}Li resonance at −274 ppm with a relative signal intensity of approximately 3%. Both of these defects will result in apparent Li/Ru exchange when probed by X-ray and neutron diffraction. The latter type of defect is an extreme example of the former, where the size of the anti-site domain corresponds to the size of the crystallite. The TEM images are consistent with the presence of a limited number of stacking faults/large anti-site domains (Figure 10). However, insufficient TEM images have been acquired to determine the size of the anti-site domains, and it is possible that both types of defects are present.

The magnetic susceptibility (Figure 12) of $La_2Sr_2LiRuO_8$ shows clear evidence of a transition at 85 K. These data, together with the displacement of the hysteresis loop observed at 5 K and the neutron diffraction data, show that the low-temperature phase is antiferromagnetic, but that a small number of spins do

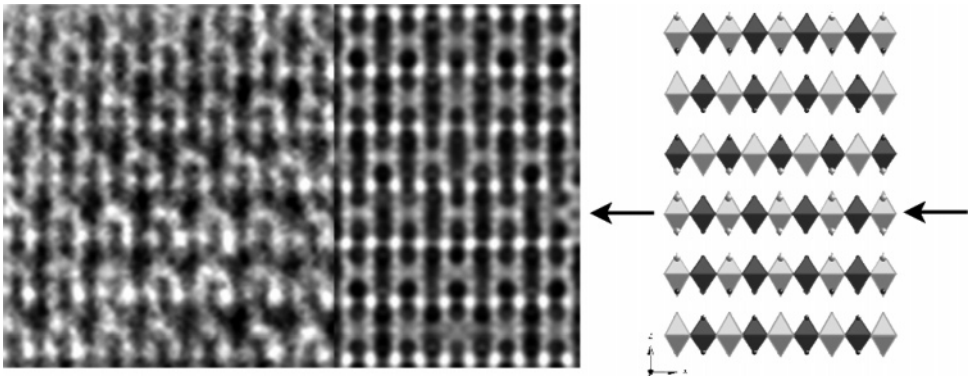

Figure 10. Detail from a [010] lattice image of $La_2Sr_2LiRuO_8$ showing an inverse Li/Ru distribution within one layer, described on the right as a relative displacement of the layer. The lattice simulation was generated using a defocus of 28 nm and a thickness of 5.6 nm.

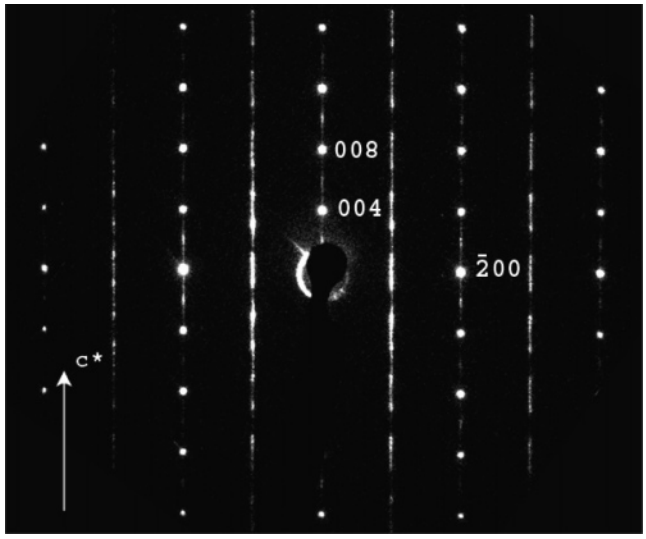

Figure 11. Selected-area [010] electron diffraction pattern of a less-crystalline area of the sample of $La_2Sr_2LiRuO_8$.

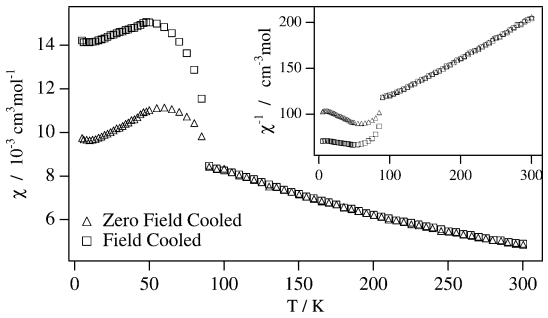

Figure 12. Molar magnetic susceptibility of $La_2Sr_2LiRuO_8$ as a function of temperature; the inverse susceptibility is shown in the inset.

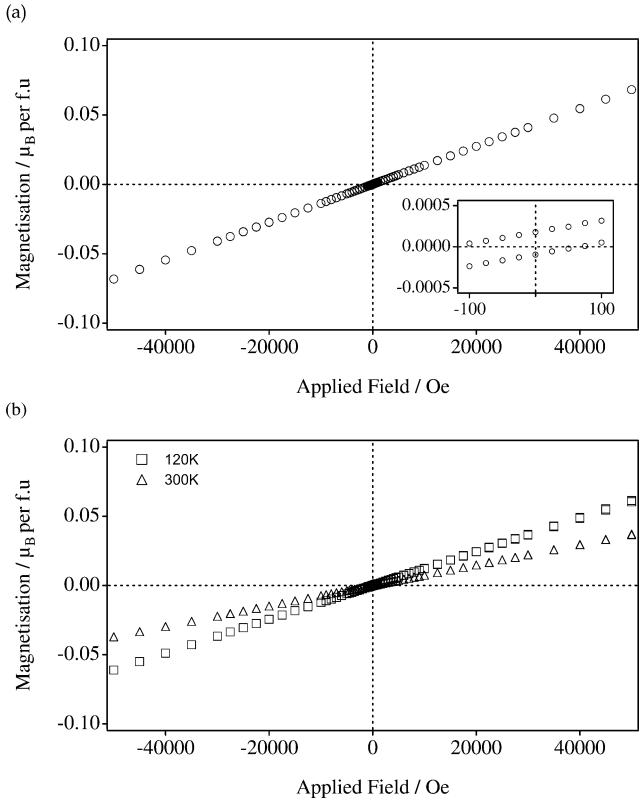

Figure 13. Magnetization of $La_2Sr_2LiRuO_8$ as a function of applied magnetic field at (a) 5 K, and (b) 120 and 300 K.

not couple to the magnetic backbone and show spin-glass behavior. These are likely to be at the Ru1 and Ru2 sites, that is, the Ru cations associated with anti-site defects. The effective magnetic moment of the Ru^{5+} cations in the high-temperature, paramagnetic phase is somewhat greater than that predicted by the spin-only formula, despite the fact that, within the localized electron model, any orbital contribution would be expected to reduce the moment of a d^3 cation on an octahedral site. However, the low value of the ordered magnetic moment measured by neutron diffraction shows that a considerable amount of covalency is present in the Ru−O bonds. This covalency broadens the 4d energy band and consequently leads to a breakdown of the localized-electron model and a shift toward itinerant electron behavior. The enhanced values of the effective magnetic moment and the Weiss temperature, θ, are characteristic of this change.[21] However, the observed Néel temperature of 85 K shows that relatively strong antiferromagnetic superexchange interactions persist in this compound. Indeed, the transition temperature in two-dimensional $La_2Sr_2LiRuO_8$ is higher than that in the three-dimensional perovskite La_2LiRuO_6 (30 K).[9] The Ru sublattice in the latter compound is pseudo face-centered and therefore prone to the effects of magnetic frustration, whereas there is no

(21) Battle, P. D.; Goodenough, J. B.; Price, R. *J. Solid State Chem.* **1983**, *46*, 234.

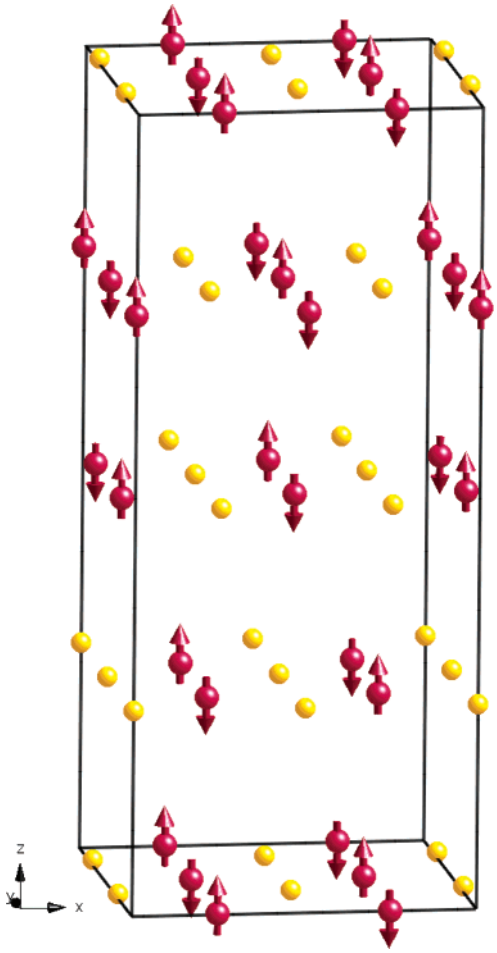

Figure 14. Magnetic structure of $La_2Sr_2LiRuO_8$ at 2 K; only Ru and Li ions are shown.

frustration in the *xy* sheets of the former and a unique ordering pattern, supporting antiferromagnetic interactions between nearest-neighbor Ru^{5+}:$4d^3$ cations, can be established. The factors that determine the spin structure along *z* are less clear, although the superexchange interactions are clearly strong enough to support a Néel temperature of 85 K. It appears that the strength of the magnetic coupling in 4d systems might previously have been underestimated because the first compounds to be studied all suffered from the effects of frustration in three dimensions.[21−24]

To conclude, $La_2Sr_2LiRuO_8$ presents a novel variation of the $n = 1$ RP structure. The compound shows some disorder at the microstructural level, but the majority of the crystallites show good coherence over the distances sampled by X-ray and neutron diffraction, and the observed unit cell is consequently doubled along [001] by cation ordering on both the La/Sr and the Li/Ru sites; the compound orders antiferromagnetically at 85 K. A number of issues arise from this research that merit further study, most obviously the factors that stabilize this structure for this particular composition and, in our hands, no other. The asymmetry of the structure also raises interesting questions concerning the dielectric properties of $La_2Sr_2LiRuO_8$. We shall report on these topics in future publications.

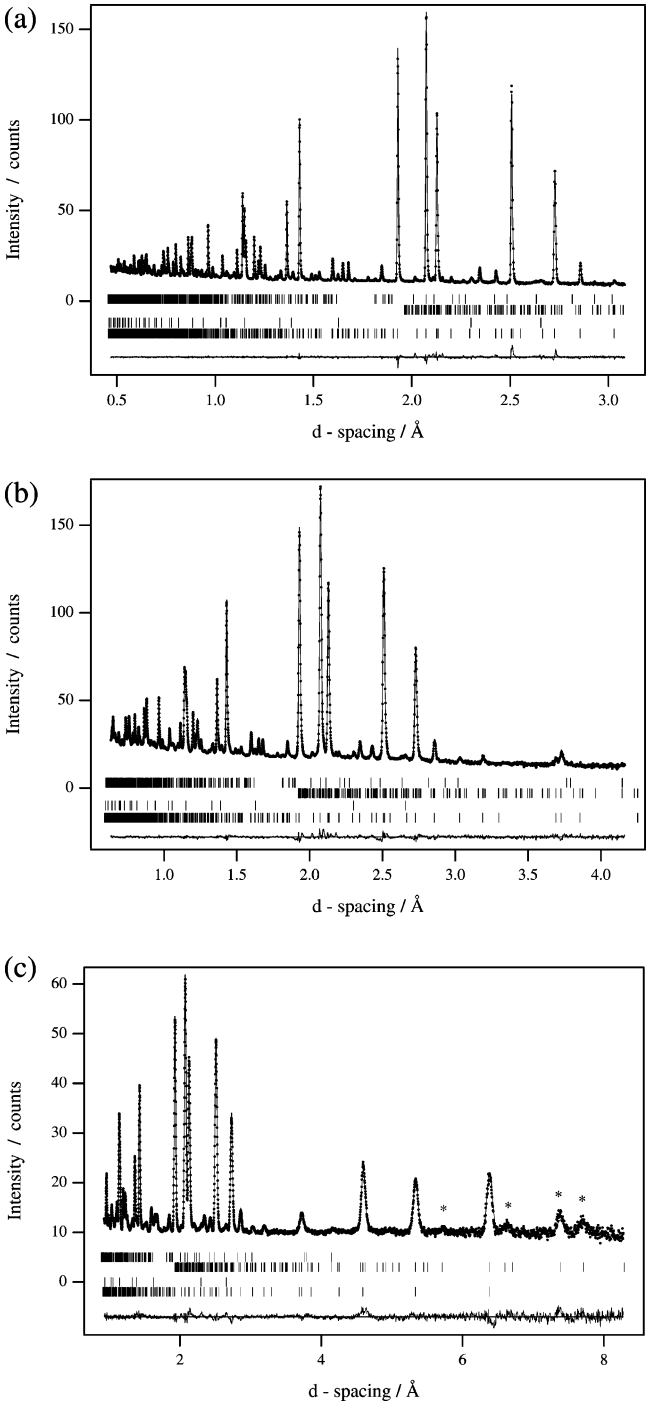

Figure 15. Observed (●), calculated (−), and difference neutron diffraction profiles of $La_2Sr_2LiRuO_8$ at 2 K collected at (a) $2\theta = 145°$, (b) $2\theta = 90°$, and (c) $2\theta = 30°$. In descending order, the tick marks refer to the magnetic structure, Li_2CO_3, Li_2O, and the crystal structure of $La_2Sr_2LiRuO_8$. Magnetic reflections are highlighted (*) in (c).

Acknowledgment. We thank EPSRC (a studentship for J.A.R.), the Royal Society (a Research fellowship for J.S.), and the NSF (via grant DMR0211353 to C.P.G.) and the Camille and Henry Dreyfus Foundation (via a Teacher-Scholar Award to C.P.G.) for financial support. We are grateful to Ron Smith for experimental assistance at ISIS.

CM049053W

(22) Battle, P. D.; Macklin, W. J. *J. Solid State Chem.* **1984**, *52*, 138.
(23) Battle, P. D.; Jones, C. W. *J. Solid State Chem.* **1989**, *78*, 108.
(24) Battle, P. D.; Jones, C. W.; Studer, F. *J. Solid State Chem.* **1991**, *90*, 302.